Review Article

Michał W. Ochapski and Michel P. de Jong*

Progress in epitaxial growth of stanene

https://doi.org/10.1515/phys-2022-0021
received November 19, 2021; accepted February 20, 2022

Abstract: With the rise of graphene, other elemental 2D materials have received a massive increase in interest in recent years. However, while theoretical models of free-standing materials predict exotic properties, often outshining those of graphene, the experimental field struggles with the synthesis of such materials. Epitaxial growth has become the main method used in experiments, as the consensus in the scientific community is that such materials require a stabilizing support. In this context, a substrate material suitable for supporting a 2D layer while preserving its topological properties is a key factor in the process. In this review article, our focus is directed to substrates for an elemental topological 2D material from group IV – stanene. We present the current state of the experimental field and give an outlook on future possibilities investigated in density functional theory (DFT) calculations.

1 Introduction

After the discovery of graphene, a two-dimensional (2D) material (single layer of C atoms) with exceptional electronic properties, interest in other 2D materials has skyrocketed. One of the most attractive properties of graphene is that its charge carriers behave as massless Dirac fermions [1], which leads to exceptionally high mobility values on the order of 10^5 cm^2 V^{-1} s^{-1} [2]. A two-dimensional (2D) topological insulator phase, the quantum spin hall insulator (QSHI), has also been predicted to exist in graphene [3]. The spin–orbit coupling (SOC) that lies at the origin of these phenomena is very weak, and hence, the effects may be observed only at extremely low temperatures [4]. Other elements of group IV, *e.g.*, Si, Ge, and Sn, exhibit the same valence electronic configuration as C, leading to similar band structures in bulk crystals, while the SOC increases strongly with atomic number Z, roughly as Z^4. This has led to enormous interest in graphene-like, 2D materials of group IV elements. While theoretical work on layered, graphite-like Si and Ge featuring corrugated atomic planes was reported in 1994 by Takeda and Shiraishi [5], the name "silicene" for the Si analog of graphene was coined in 2007 by Guzmán-Verri and Lew Yan Voon [6] in their early experimental reports on epitaxial silicene in 2012, and was used in the works of Vogt *et al.* [7], and in the works of Fleurence *et al.* [8]. Since then, the field of silicene studies has grown tremendously [9,10]. Similarly, the Ge analog of graphene – germanene – appeared in the literature in 2009 [11,12]. The first successful growth of germanene followed soon after [13] and the field has been growing since then [14–16].

Stanene, which took its name from the Latin name for tin – *stannum* [17], along with the aforementioned materials, belongs to the group-IV 2D materials family. It is a monolayer of Sn in a honeycomb, graphene-like, lattice. The interest in stanene can be regarded as a follow-up of the development of the field, in particular the research on the feasibility of the lighter group IV elements.

The investigation of stanene has started in 2013 with a seminal paper by Xu *et al.* [17], where the authors pointed out the possibility of the quantum spin Hall effect (QSHE) in stanene sheets to appear above room temperature. Another early report on the properties of free-standing stanene was by Broek *et al.* in 2014 [18]. While the first papers focused on theoretical properties and stability of such a layer, still hypothetical at the time, the first experimental work appeared only a year later – Zhu *et al.* in 2015 reported on stanene on Bi_2Te_3 [19]. As in the case of the other elemental 2D materials, the field grew rapidly with time, and by now, stanene is a material with a well-established theoretical base, which powered the expanding experimental aspect of the research. There is a number of review papers that summarize well the properties of stanene [20–22]. Unlike these review articles, this work focuses on the summary of the experimental realization of stanene *via* epitaxial growth – the most popular and most promising method of fabricating the

* **Corresponding author: Michel P. de Jong,** MESA+ Institute for Nanotechnology, University of Twente, 7500 AE Enschede, The Netherlands, e-mail: M.P.deJong@utwente.nl
Michał W. Ochapski: MESA+ Institute for Nanotechnology, University of Twente, 7500 AE Enschede, The Netherlands; Center for Nanotechnology Innovation @ NEST, Istituto Italiano di Tecnologia, Piazza San Silvestro 12, 56127 Pisa, Italy

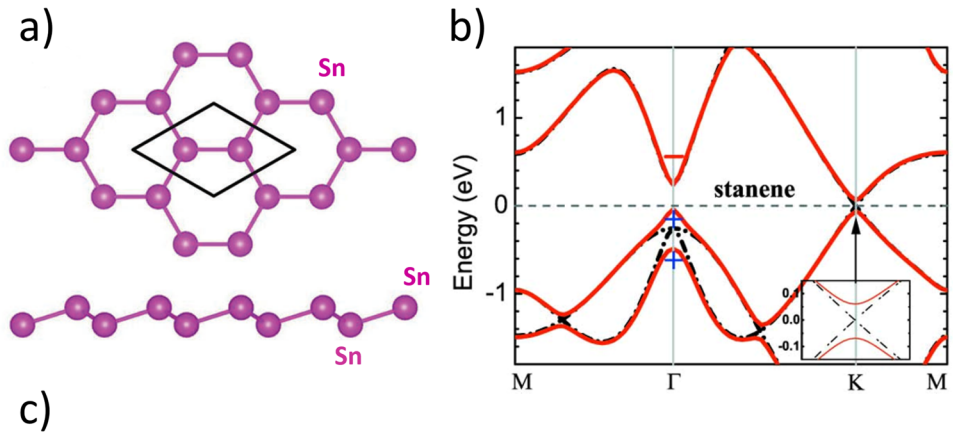

	C	Si	Ge	Sn
a (Å)	2.468	3.868	4.060	4.673
d (Å)	1.425	2.233	2.344	2.698
Δ (Å)	0.00	0.45	0.69	0.85
v_F (10^6 m s^{-1})	1.01 (0.83)	0.65 (0.53)	0.62 (0.52)	0.55 (0.48)
m^* (m_0)	0.000 (0.000)	0.001 (0.001)	0.007 (0.008)	0.029 (0.028)
E_g (meV)	0.0 (0.0)	1.9 (1.5)	33 (24)	101 (73)

Figure 1: (a) Top and side views of the stanene lattice with primitive cell indicated by black rhombus. Stanene is a homogenous monolayer of Sn, with two chemically equivalent sublattices (upper and lower). (b) Electronic band structure of stanene without (black dash-dotted lines) and with (red solid lines) SOC. The inset shows a zoomed-in energy dispersion near the K point. The Fermi level is indicated by the dashed line. One can see the Dirac cone at the K point. The observed band inversion at the K point and a band gap opened by the SOC, indicating nontrivial topological properties of the material. (c) Comparison of the structural and electronic parameters of group IV elemental 2D materials. From the top: lattice constant a, bond length d, buckling parameter Δ, Fermi velocity v_F, effective masses of Dirac particles m^*, electronic band gap E_g. Electronic quantities are derived from hybrid HSE06 calculations. The general gradient approximation (GGA) results are given in parentheses. E_g and m^* are calculated with the inclusion of SOC (without SOC, $E_g = m^* = 0$). Reproduced from (a) [28], (b) [17], and (c) [29].

material up to date. We hope this review to be a complementary source of information, especially for new researchers in the field.

2 Structural stability

Like the other novel 2D materials from group IV, stanene has a buckled honeycomb lattice structure with two atoms in the primitive cell. The lattice constant has been initially reported to be 4.62–4.68 Å [17,18]. Sn atoms are relatively large in comparison with the lighter group IV elements. This gives rise to the effects, which make stanene a very interesting material. One such effect is the buckling of the lattice. The repulsion forces between Sn atoms are relatively strong, which results in larger bond lengths (~2.69 Å compared to graphene ~1.42 Å) that prevent the atoms from forming strong π bonds. Sn atoms are pushed in the out-of-plane direction, effectively buckling the lattice and deviating the structure away from pure sp^2 into a mixed sp^2–sp^3 hybridization.

The other distinguishing effect present in stanene is nonnegligible SOC, which makes it a topological insulator [17,23], analogous to the initial prediction of a QSHI state by Kane and Mele [3]. The SOC is much stronger than in C, Si, or Ge due to the larger nuclear charge of Sn atoms. In addition, the hybridization between the π and σ orbitals of nearest neighbors becomes allowed in a buckled structure. This allows for an additional first-order contribution to the SOC [24–26]. Therefore, the SOC-induced gap at the K and K′ points, which lies at the heart of the formation of the QSHI state, is much larger and has been predicted to surpass the thermal energy even at room temperature. In total, larger atomic mass and the buckling of the lattice increase the QSH gap in stanene by five orders of magnitude with respect to graphene [24].

These effects have far-reaching consequences and are the main characteristics that distinguish stanene from graphene. Similar effects are found in silicene and

germanene [12]. However, in the case of Sn atoms, as the largest among the three, the effects and resulting phenomena are the strongest.

In free-standing stanene, like silicene and germanene, there are two energy minima classified according to buckling height Δ as high (HB) and low (LB) buckling of the lattice. Calculations of stability suggest that, in contradiction to silicene and germanene, the HB phase is the global minimum with a lattice constant of 3.4 Å [27]. However, that phase is metallic. Hence, the interest is mainly in the LB phase, which is predicted to have nontrivial topological properties [17]. In the LB phase, stanene has the lattice constant of 4.68 Å and buckling height of Δ = 0.85 Å [17]. Figure 1a and c show the atomic structure of free-standing LB stanene as well as its predicted structural parameters. Another form of a free-standing monolayer of Sn is dumbbell stanene, which is also calculated to be more stable than the LB phase [30]. However, this structure is far from the graphene-like configuration, and hence, it is not going to be discussed further in this review.

3 Properties

Many theoretical studies have been done on a variety of properties of stanene. Here, we shortly summarize its most important electronic characteristics, as these draw the most attention to the material. The two most important features recognized in its band structure are the preservation of the linear energy dispersion (Dirac cones) at the K and K′ points, which signalize high carrier mobility, as well as a significant SOC-induced band gap of 100 meV [17], which predicts stanene to be a topological insulator and allows for a quantum spin Hall effect (QSHE) to occur at room temperature [31]. This seems to be the largest nontrivial band gap for a free-standing 2D material of group IV, as Pb – the heaviest group IV element – in its 2D form is a metal [17]. The band gap can be further tuned and enlarged by various techniques, such as chemical functionalization [32], strain [28,33], or electrical field [34,35] up to 0.3 eV [17]. Figure 1b and c give insight in stanene's electronic properties.

4 Substrates

Experimental realization of stanene (as well as silicene and germanene) is problematic due to sp^3 hybridization being energetically more favorable than sp^2. As a result, there is no layered form of Sn analogous to graphite in nature. The solution to this obstacle is the synthesis of a substrate that would support the formation of a Sn monolayer. The main challenge in this approach is the choice of a suitable substrate. There are a few properties that a substrate should possess to be a promising candidate. First, the stanene – substrate heterostructure must be stable. The stability is ensured in two ways – hexagonal or honeycomb symmetry of the outermost layer of the substrate and small lattice mismatch, to minimize the strain in the Sn layer. Second, the electronic properties of free-standing stanene have to be preserved. To achieve this, preferable substrates must have a band gap as well as have to interact weakly (*via* Van der Waals forces) with the 2D material. Therefore, layered semiconductors or insulators with matching lattice constants would be perfect candidates *a priori*.

4.1 Substrates with reported realization of epitaxial of stanene

Several substrates have been examined theoretically for their feasibility to support stanene and preserve, or possibly even enhance, its properties. We note in passing that Sn growth on various substrates has been studied for a long time. Only recently, thanks to the rise of graphene and the prediction of the exotic properties in analogous 2D materials, the attention was directed to the quantum physical properties of Sn sheets.

4.1.1 Bi_2Te_3

The first report calling an epitaxial multilayer of Sn "stanene" has been reported in 2015 by Zhu *et al.* [19]. The Sn layer was epitaxially grown on Te-terminated bismuth telluride (Te-Bi_2Te_3) (see Figure 2a). The growth was characterized by the Vollmer-Weber mode (island growth). While the structural properties were in close accordance with the predicted values, the electronic band structure was strongly influenced by the substrate. The report opened the field of epitaxially grown stanene-like structures. Motivated by that successful experimentally realized growth, systematic DFT calculations of the system by Zhang *et al.* suggested that growth on the Te-terminated Bi_2Te_3 surface follows a partial-layer-by-partial-layer (PLBPL) growth mode, characterized by short-range repulsive pairwise interactions of the Sn adatoms. They

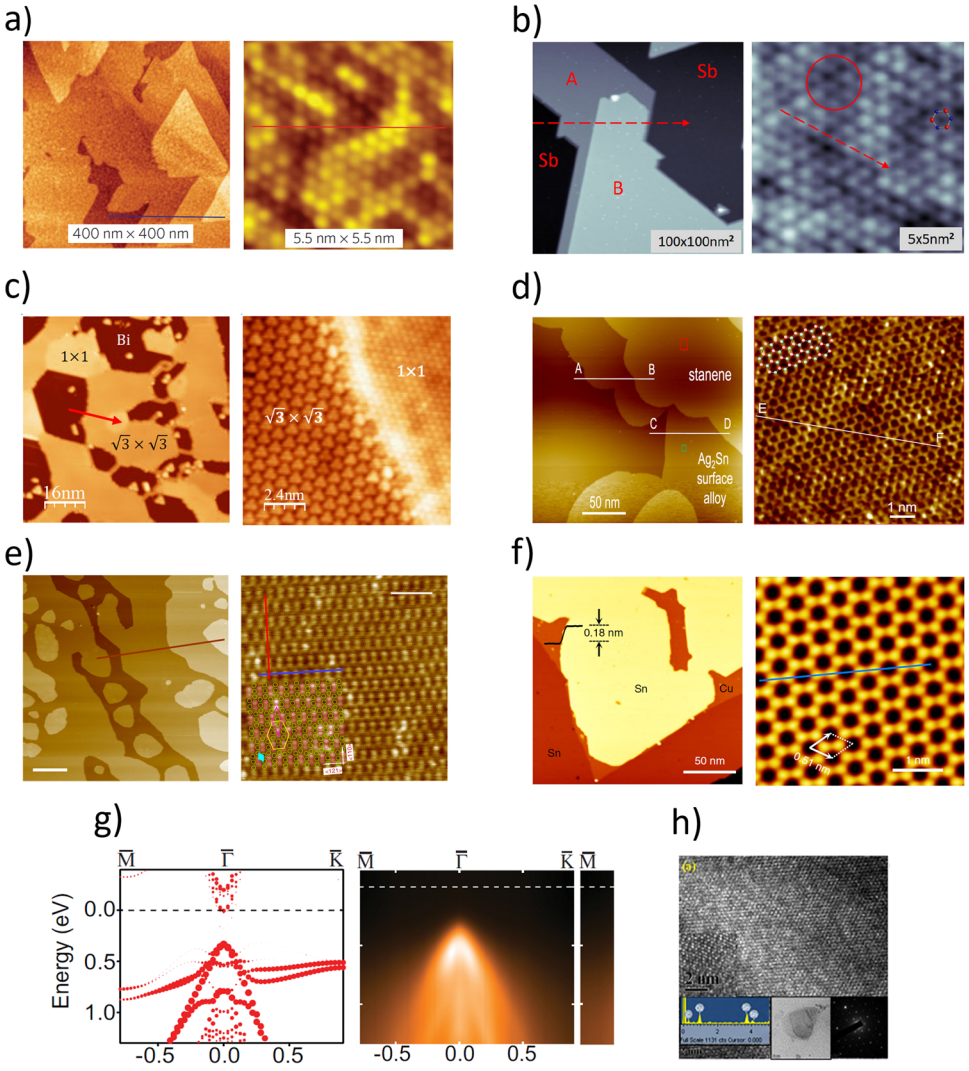

Figure 2: (a–f) Selected large area and high-resolution STM images of epitaxial stanene grown on: (a) Bi_2Te_3, (b) Sb(111), (c) Bi(111), (d) Ag_2Sn surface alloy, (e) Au(111) (f) Cu(111), and (g) band structure of stanene on InSb, calculated (left) and measured with ARPES (right). (h) High – resolution transmission electron microscopy (HRTEM) image of a free-standing Sn layer showing a hexagonal lattice. Reproduced from (a) [19], (b) [46], (c) [47], (d) [57], (e) [64], (f) [65], (g) [63], and (h) [66].

proposed that Bi_2Te_3 precovered with a Bi bilayer would support the nucleation and growth mechanism, strongly favoring single-crystalline stanene [36]. Finally, a critical view on the possible growth of stanene with its expected properties on this substrate was signaled recently by Li *et al.* [37]. In their investigation of the electronic band structure of that system by X-ray photoelectron spectroscopy (XPS) and angle-resolved photoelectron spectroscopy (ARPES), they showed a significant interfacial chemical interaction between Sn atoms and Bi_2Te_3. The presence of this interaction, leading to Sn – Te chemical bonds in the stanene/Bi_2Te_3 system, casts doubts on the feasibility of this substrate for the stanene growth.

4.1.2 Al compounds

Other substrate materials that appear in the literature are Al and several Al compounds. The pure Al(111) surface was predicted to support buckled, metallic stanene [38]. However, the high-resolution scanning tunneling microscopy (STM) image for Sn monolayers on Al(111) exhibits a square-like structure [39]. Among compounds containing Al, aluminum oxide α-(Al_2O_3)(0001) was investigated theoretically by DFT and tight-binding methods. Araidai *et al.* [40] reported that the electronic structure of the adsorbed stanene strongly depends on the stanene – alumina distance, which alters the influence of

Sn–O bonds of antibonding nature (see Figure 3a). The band splitting induced by the Rashba effect was observed by taking into account the spin–orbit interactions. Stanene on α-alumina did not show the electronic state characteristic for two-dimensional honeycomb sheets, according to the authors. However, there is still the possibility of a QSHE at room temperature due to the substrate effect according to Wang *et al.* [44]. They report a large topologically nontrivial band gap, up to 0.25 eV. A more recent work by Eltinge and Ismail-Beigi [45] also explores the structural and electronic properties of stanene on $Al_2O_3(0001)$ by means of DFT. Their results confirm previous models and possible topological properties of stanene on Al_2O_3. Finally, aluminum nitride (AlN) has been examined theoretically by DFT calculations [28]. The authors calculated the influence of external strain on the stanene/AlN heterostructure. By calculating the electronic structure for different configurations, the authors concluded that a QSHE can be induced in the low external strain regime, while the nontrivial topological properties were lost at high external strain.

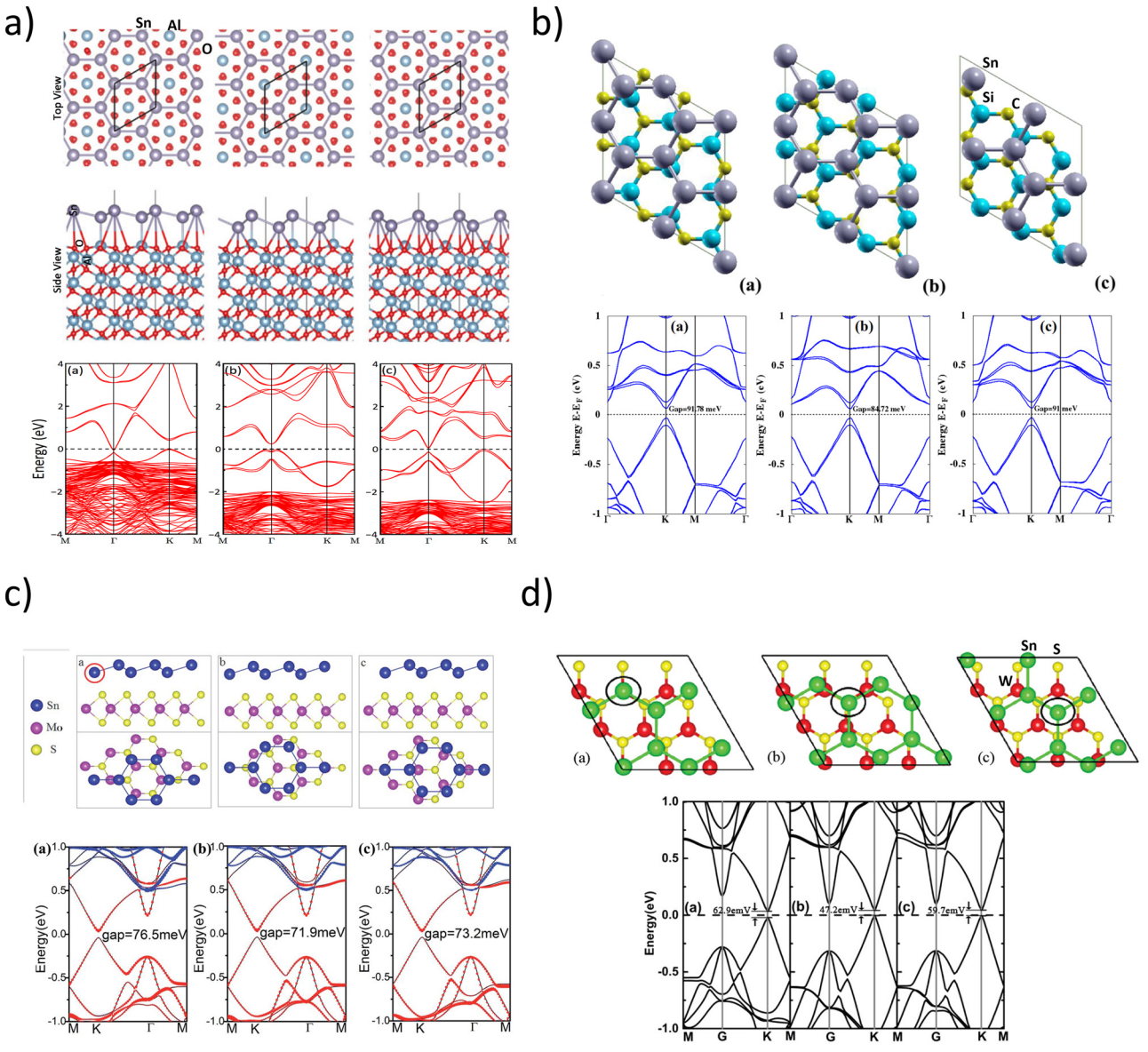

Figure 3: (a) Proposed atomic configurations of stanene on α-Al_2O_3 (0001) in top and side views, and their calculated band structures, including SOC. In the side view, the bonds between atoms are added in each configuration. (b) Stanene on SiC in three configurations with the corresponding calculated band structures with SOC. (c) Stanene/MoS_2 stacks and their band structures with SOC. (d) Stanene/WS_2 stacking configurations and corresponding calculations of their band structures. Figures reproduced from (a) [40], (b) [41], (c) [42], and (d) [43].

4.1.3 Sb(111)

An interesting experiment with a similar substrate was undertaken by Gou *et al.* [46], who report on an epitaxially grown stanene film on an antimony (Sb(111)) substrate (see Figure 2b). The significant stress that the stanene layer undergoes widens the band gap at the K points to 0.2 eV, which is twice as big as the predictions for the freestanding material. However, multiple bands cross the Fermi level at the Γ point making stanene metallic. A systematic investigation with scanning tunneling spectroscopy (STS) proved that the stanene band structure can be tuned with strain.

4.1.4 Bi(111)

In their article, Song *et al.* [47] presented their work on stanene growth on Bi(111). STM measurements showed that, apart from low buckled 1×1 stanene, they also obtained a highly buckled $\sqrt{3} \times \sqrt{3}$ formation (see Figure 2c). Upon closer look by means of STM, STS, and DFT calculations, they concluded that the new formation is a 1×1 lattice, distorted with a high-buckled atom in every third unit cell. Interestingly, the STS measurements detected the edge states, and DFT calculations showed that the spin–orbit coupling opens a topologically nontrivial energy gap at the Γ point. Unfortunately, the gap is above the Fermi level, such that to utilize topological properties, additional tuning of the Fermi level is required.

4.1.5 PbTe(111)

In their study from 2018, Zang *et al.* [48] report on stanene grown on Sr-doped lead telluride (Sr-PbTe(111)). The Sn layer was unintentionally passivated by H, despite being kept in an ultra-high vacuum (UHV) environment. While the obtained stanene seemed to be a trivial insulator, the authors suggest activating the topological properties by stretching its lattice constant, which, as they further imply, can be done using similar substrates, like EuTe, SrTe, and BaTe with larger lattice constants. At about the same time, PbTe-covered Bi_2Te_3 was used by Liao *et al.* to grow few-layer stanene films, which revealed novel superconducting behaviors controlled by the number of Sn layers [49].

4.1.6 SiC

Glass *et al.* investigated silicon carbide (SiC) substrates and reported the first realization of a triangular Sn lattice on SiC(0001) [50]. STM revealed the structure of the Sn lattice, which was reproduced in DFT calculations. DFT predicted a Sn-related band to cross the Fermi level, in the middle of a large band gap. Additional UPS measurements suggest a Mott-insulating state. Encouraged by this promising result, Matusalem *et al.* [51] showed in their calculations that the passivation of the substrate and Sn layer in the stanene/SiC system results in quasi freestanding overlayers, with the presence of linearly dispersing Dirac-like bands in the band structures. They also identified the configuration in which stanene conserves its topological character. Another variation proposed by the same group was a graphene-covered SiC substrate [52]. In this case, while the Dirac cone is conserved, the authors report on strong charge transfer from stanene to graphene, which makes the topology of the system unclear. The possibility of substrate engineering was significantly explored by Di Sante *et al.* [53], who analyzed the influence of an elemental buffer layer on the stanene/SiC system. The buffer layers they examined were elemental Group III and V lattices. The goal was to protect the QSHI state in stanene. They chose atoms that have their bonding and antibonding states energetically far away from the chemical potential to minimize the detrimental staggered potential (due to lifting sublattice degeneracy). The analysis made them propose P and As the best candidates for buffer layers. While other attempts focused on adding additional layers to tune the substrate, Ferdous *et al.* [41] investigated the properties of a stanene/SiC heterobilayer (see Figure 3b). That system manifests a wide band gap up to 160 meV at the K point with a well-preserved Dirac cone. A closer look at the topological properties of stanene on SiC was undertaken by Li [54]. In their calculations, stanene was stabilized by the strong interfacial bonding. This resulted in quadratically dispersing (non-Dirac) topological states at the Γ point, constructed of stanene's $p_{x,y}$ orbitals, instead of the p_z orbitals that are normally involved in such states.

4.1.7 Ag(111)

After the successful growth of silicene on Ag(111), this became another candidate substrate for the possible growth of monolayer Sn. Ag was one of the metals investigated in the theoretical work of Guo *et al.* [38] about the interfacial properties of stanene on various metals. They concluded that, while stanene is structurally stable on Ag and some of the other metals examined, it undergoes metallization on all of them. Further theoretical insight into the structural stability of the stanene/Ag(111) system was given by

Gao *et al.* [55]. They showed that there are four stable reconstructions, which could revert to the free-standing structure upon removal of the Ag substrate. They suggested that it is a good candidate for a proof-of-principle transistor, similar to the silicene-made device, which was made by etching away Ag without destruction of the overlayer [56]. Inspired by theory, Yuhara *et al.* [57] reported on the growth of large area planar Sn-sheets on Ag(111) (see Figure 2d). Upon deposition of 1/3 of a monolayer (ML), an Ag_2Sn alloy is formed. Further deposition gave rise to an additional planar layer of Sn. ARPES measurements identified the heterostructure as metallic. The formation of an alloy layer poses a question about the possibility to remove the substrate to obtain a free-standing material, like in the case of silicene. An attempt to solve this problem was undertaken by Luh *et al.* [58] who performed a temperature-dependent study on the Sn growth on Ag(111). Inspired by the previously calculated large diffusion coefficient for Sn on Ag(111) at 300 K, they conducted Sn deposition at lowered temperatures to prevent forming an alloy. However, they failed to achieve this even at temperatures as low as 96 K. The question if there is an alloy-free regime below that temperature in the Sn/Ag systems remains unanswered for now.

4.1.8 InSb(111)

Indium antimonide (InSb) has been regarded as a promising candidate for the growth of Sn sheets [59–61]. Barfuss *et al.* [62] reported the possibility to obtain a quantum 3D topological phase in strained α-Sn on this substrate. They also predicted the QSHE in a Sn monolayer on this substrate. Another argument for the feasibility of this material to support a stanene layer was provided by Tang *et al.* [30]. In their article, Tang *et al.* investigated dumbbell stanene on the InSb(111)-(2 × 2) thin film and concluded that, despite strong coupling between the substrate and the Sn layer, the topologically nontrivial properties persist in the hybridized structure, such that DB stanene is a 2D TI without inversion symmetry. Finally, Xu *et al.* [63] reported on stanene epitaxially grown on InSb(111)B (Sb terminated) (see Figure 2 g). ARPES measurements of the pristine films and K-doped films demonstrate a large gap of 0.44 eV at the Brillouin zone center. The size of the band gap – 0.440 eV – is larger than that expected for freestanding stanene because of the electronic coupling between the Sn and InSb conduction band states [63]. Such a large band gap suggests the exotic properties in this structure to be accessible even above room temperature (for T = 300 K, the thermal energy k_BT is 0.026 eV).

4.1.9 Au(111)

Nigam *et al.* [67] investigated the Au(111) surface as a potential candidate for a substrate supporting stanene *via* DFT calculations. The Sn layer prefers a planar over a buckled structure, which was explained by the participation of Sn–p_z orbitals in bonding with Au. This is contradictory to the work by Guo *et al.* [38], who in their calculations obtained buckled stanene on Au(111) with a buckling parameter almost twice bigger than in the case of free-standing stanene. The authors realized this discrepancy and suggested considering different Van der Waals corrections [38] as the possible reason. Experimental realization of stanene on Au(111) was achieved by Liu *et al.* [68]. The deposited Sn atoms first formed a surface Sn–Au alloy, with a coverage-dependent structure. Upon further deposition, above a critical coverage, the Au–Sn alloy was converted into a strongly buckled, disordered honeycomb lattice of epitaxial stanene. DFT calculations and STM images suggest strong tensile strain in the layer. Maniraj *et al.* [64], after their initial report on the same alloy [69], also reported on stanene formation on Au(111) (see Figure 2e). Their ARPES investigation showed that the band structure of the Sn/Au superstructure is dominated by a linearly dispersing band centered at the Γ point, corresponding to a high Fermi velocity and a spin texture of a three-dimensional topological insulator. Pang *et al.* [70] in turn, presented new Sn formations on a Au(111) surface, examined by low-energy electron diffraction (LEED) and STM, which showed an unusual reconstruction, most probably due to uniaxial compression of the Au surface along the [110] direction. The structure is flat and reveals a distorted hexagonal symmetry. Interestingly, while XPS suggests the presence of an Au-Sn alloy, typical for this system, no trace of alloy-related bands are detected in ARPES measurements. The authors proposed zigzag chains and honeycomb-like structures based on the experimental results and DFT calculations. Finally, Zhou *et al.* [71] in their recent report explored the phase space of Sn formations on an Au_2Sn alloy. Their investigation reveals a set of temperature-dependent reconstructions. Apart from a hexagonal stanene-like structure, they found also Sn tetramers and clover-shaped Sn pentamers as well as, observed for the first time, a black-phosphorus-like Sn layer.

4.1.10 Cu(111)

A similar example of a planar Sn layer was reported on Cu (111) by Deng *et al.* [65] (see Figure 2f). The method used

to prevent forming an alloy was deposition at low temperature, in this case 200 K. The obtained structure was an atomic layer of Sn in a planar honeycomb lattice with no buckling, which was named "ultraflat stanene." The strong interactions with the substrate and the lattice stretching stabilized the zero – buckling geometry, creating a honeycomb lattice. This lattice was characterized by an s–p band inversion and a band gap at the Γ point induced by SOC. Green's function calculations confirmed the topologically derived boundary states suggested by STS measurements. The structure is stable up to 240 K. It is also important to note that even though there was a finite band gap in the stanene layer, ARPES measurements showed that the system was overall metallic due to metallic bands from the substrate. Ahmed *et al.* [72] presented the further structural analysis of the stanene layer by means of LEED and DFT. Their analysis suggests that the ultraflat character of stanene was induced by a horizontal and vertical relaxation of the outermost layers of the Cu(111) substrate. Even though the vertical displacements of the two Sn atoms at different adsorption sites have been found to differ slightly in the calculations, the low Debye temperature and the resulting vibrations corresponding to a high error range reduce the difference to below the experimental detection limit.

4.1.11 MoS_2

Reports on experimentally realized growth of silicene [73,74] and germanene [75] on molybdenum disulfide (MoS_2) gave hopes for utilizing the material as a substrate also for the epitaxial synthesis of stanene. Liang *et al.* [76], Xiong *et al.* [77], and Ren *et al.* [42] (see Figure 3c) reported, at approximately the same time, very similar studies on the stability and electronic properties of a stanene/MoS_2 heterobilayer using DFT. A band gap was opened at the K point (slightly shifted in the case of Ren *et al.*) due to MoS_2 breaking the symmetry of the sublattices of stanene (slightly bigger in the case of Xiong *et al.* than in the other two reports). In the case of Liang *et al.* and Ren *et al.*, the Dirac cone was preserved, while Xiong *et al.* report on electron transfer from stanene to the substrate forming an internal electric field. The Dirac cone recovers upon applying an external field, equal to the internal one. The reason for the discrepancies may come from a different optimal interlayer spacing calculated, different stacking patterns as well as different functionals used in the calculations. All three reports conclude that the band gap can be effectively tuned with external strain and electric field. In the experimental field, although Chen [78] reports on forming multilayer stanene on MoS_2, the thickness of the deposited layer was 100 nm. This poses a question if the name "stanene," which refers to an atomic monolayer of Sn, is used appropriately, as the experimental measurements in the paper are limited to transmission electron microscopy (TEM) and X-ray diffraction (XRD), while atomic force microscopy (AFM) images are not atomically resolved.

4.1.12 Graphene

An interesting idea is to combine two or more elemental 2D materials together. Chen *et al.* [79] explored that idea by investigating a stanene/graphene heterostructure. They studied structural, electronic, and optical properties of several stacking configurations by means of DFT. They found interactions between the layers being stronger than typical Van der Waals bonds, which improves the stability of the system. In the case of some stacking configurations, the system exhibits a Dirac feature in the vicinity of the K point. The authors suggest the tunability of the gap by means of an electric field. Finally, the system showed enhanced visible light absorption in all configurations. Wu *et al.* [80] performed similar calculations, additionally showing that multiple crystalline phases can coexist at room temperature (see Figure 4a). They also suggest the possibility of tuning the electronic properties. Yun *et al.* [82] took a closer look on that aspect and calculated the behavior of the stanene/graphene system under strain and the influence of water vapor adsorption. In their stability studies, they report an additional stacking configuration, not mentioned in the previous studies. They concluded that the Fermi level can host Dirac or parabolic bands (or a mixture of both) depending on the strain and rotation. They also selected configurations in which a gap can be opened by the application of external stress. The calculation on water vapor adsorption showed that it will modulate conductivity but not distort the band structure significantly. Another combination of stanene and graphene together was proposed by Mondal *et al.* [83] who proposed stanene sandwiched between two graphene layers. The structure exhibits a topologically protected hybrid state at the stanene–graphene interface, which is robust against severe strain. A work of Wu *et al.* [84] reported on an experimentally obtained ultrathin 2D Sn layer on graphene-covered Cu (111). While a surface coverage of a few layers graphene resulted in Sn clustering, a monolayer graphene (MLG) gave a homogenous layer of Sn. This was consistent with their calculations, in which the Sn/MLG/Cu(111) stack was the most stable. The DFT calculations and XPS measurements showed that the presence of graphene prevents strong

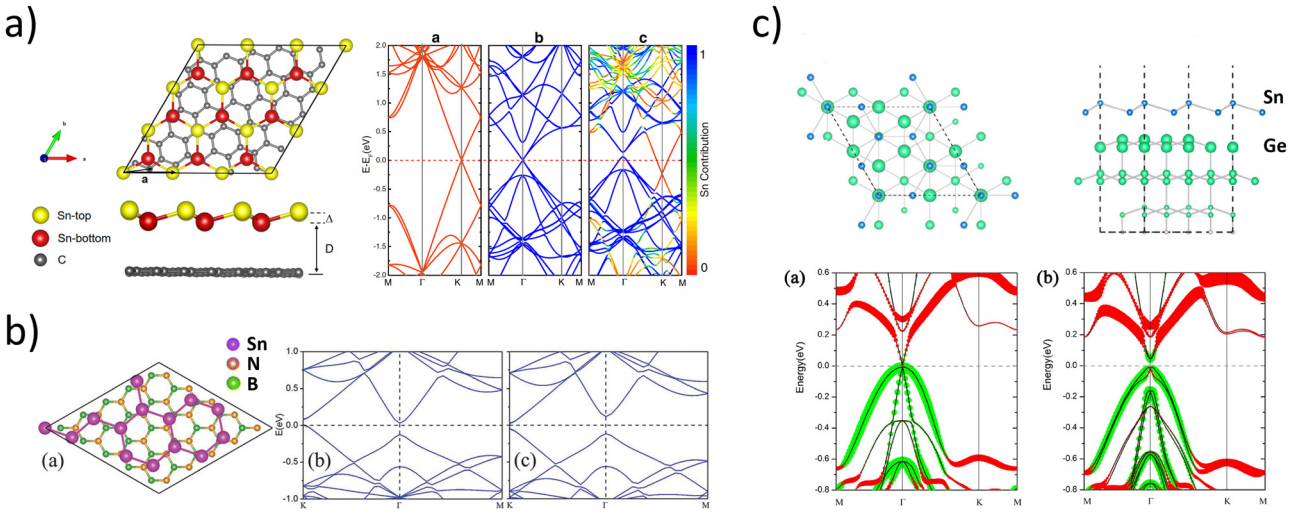

Figure 4: (a) Stanene on graphene with band structures of (from left to right) graphene, stanene, and the whole system. (b) Stanene/hBN heterostructure with corresponding band structure without (left) and with (right) SOC. (c) Model of the stanene/Ge(111)-(2 × 2) heterostructure and the band structure without (left) and with (right) SOC. Figures reproduced from (a) [80], (b) [28], and (c) [81].

hybridization between Sn and the Cu(111) substrate. Interestingly, the structure is remarkably resistant to oxidation. Unfortunately, in the experimental part, only reflection high-energy electron diffraction (RHEED) patterns giving structural information are shown, but no atomically resolved microscopy images were presented. Another interesting approach came from Yang *et al.* [85]. They presented an experimental realization of an idea to make stanene membranes in pores in graphene layers. The deposited Sn atoms formed a planar 2D clusters/patches made of up to eight Sn atoms in graphene pores. The DFT results imply that the pores can stabilize Sn atoms through interactions with the pore edges.

4.1.13 hBN

Hexagonal boron nitride (hBN), as an insulator with Van der Waals structure, was an obvious candidate for a stanene substrate. A theoretical study on the stability and the effect of strain was undertaken by Wang *et al.* [28] (see Figure 4b). They showed that stanene is stable on hBN and slightly compressed with respect to its free-standing form, which makes it semi-metallic. However, by the application of an external strain, a QSHI phase can be induced. In addition, the authors found another configuration with smaller lattice mismatch, which exhibits a QSHI phase without any strain. Another theoretical configuration was proposed in the paper of Wang *et al.* [86]. The result suggests that hBN can support stanene and preserve a topological gap. Khan *et al.* [87] also reported on a stanene/hBN heterobilayer in their theoretical work. The authors propose yet another stable configuration, in which the stanene layer is slightly stretched. The band structure of the Sn/hBN heterobilayer shows a direct band gap of about 30 meV at the Fermi energy, while the linear Dirac dispersion relation is maintained. Tensile strain and interlayer distance also have an impact on the band structure, showing that it is very prone to tuning. DFT studies on hexagonal nitrides (AlN, GaN, and hBN) as stanene substrates were also performed by Yelgel [88]. In the case of hBN, the author reported that the Dirac cone in monolayer stanene adsorbed on hBN was preserved. The partial density of states confirms the previous claims that the carrier transport occurs only through the stanene layer. The biggest band gap was calculated in the case of the stanene/GaN heterostructure. AlN shows strong interaction with the stanene layer, confirmed by the previous reports. From the experimental side, the work of Dong *et al.* [89] reports on obtaining ordered Sn phases on hBN/Ir(111). The presence of hBN altered the initially obtained results of Sn deposition on Ir(111) giving rise to a new reconstruction. An interesting phenomenon was observed, where the new reconstruction is supposedly templated by the hBN/Ir(111) Moiré pattern. STS measurements suggest the new Sn adlayer is of metallic nature.

4.1.14 Non-epitaxial stanene

While epitaxial growth is the common way to approach the synthesis of stanene, Saxena *et al.* [66] took a different

path and reported growing a freestanding few-layer stanene film, obtained by impinging pulses from a tunable Ti:Saphire ultra-fast femto-second laser onto a target in a liquid medium (see Figure 2h). They performed a series of structural studies that seem to confirm the claim; however, no electronic properties measurements have been reported so far. Their further report confirms stanene's structural signature in optical measurements [90] (Table 1).

4.2 Substrates theoretically predicted to support epitaxial stanene

There are several more theoretical papers on different substrates that are predicted to support stanene. Up to now, there has been no experimental realization of stanene on any of them reported in the literature.

4.2.1 Ge(111)

The germanium (Ge(111)) surface was examined by Fang *et al.* [81] by means of DFT calculations (see Figure 4c). They showed that stanene on Ge(111) has nontrivial topological phases. The Dirac cone exists around the Γ point, and the SOC opens up a band gap. In their report, Bachra *et al.* [91] presented detailed calculations on stability, proving that buckled stanene is the preferable phase. They also suggested that there is a strong interaction between the Sn layer and the substrate. They confirmed that stanene preserves nontrivial topological features. While the theoretical field seems to paint a tempting landscape for further exploration, the experimental reports on Sn/Ge(111) heterostructures suggest that a Sn adlayer that is rather different from stanene is formed [92,93].

4.2.2 InSe and GaTe

Ding and Wang [94] proposed InSe and GaTe as other candidates for stanene substrates. In their paper, they calculated that stanene is stable on both of the substrates and preserves its Dirac cone as well as the SOC-induced band gap.

4.2.3 Survey of metallic substrates

Guo *et al.* [38] surveyed several metallic substrates using DFT, including the aforementioned Ag, Au, Cu, Al, as well as Pd, Pt, Ir, and Ni. The stability of the honeycomb lattice was preserved; however, buckling parameters changed depending on the substrate. They also reported on the destruction of the stanene band structure and its metallization for all the substrates examined.

4.2.4 PbI_2

Zhang *el al.* [95] reported calculations on a functionalized stanene/PbI_2 heterostructure as a suitable system for observing the quantum anomalous hall effect (QAHE). The substrate is nonmagnetic; therefore, they induced ferromagnetism in the structure *via* functionalization of stanene. They also proposed a device comprising stanene

Table 1: Substrates on which stanene growth has been reported

Substrate	Substrate electronic properties	Reconstructions	Λ (Å)	*d* (Å)	Ref.
Bi_2Te_3	Topological insulator	1×1	4.4	3.5	[19]
Free-standing	No substrate	1×1	4.7	3.3	[66]
Sb(111)	Semimetal	1×1	4.3	—	[46]
Cu(111)	Metal	2×2	5.1	1.8	[65]
Graphene/Cu(111)	Semimetal/metal	$\sqrt{3} \times \sqrt{3}$R30	4.45	—	[84]
Ir(111)	Metal	2×2	5.5		[89]
hBN/Ir(111)	Insulator/metal	$\sqrt{7} \times \sqrt{7}$R30	7.2		[89]
InSb(111)	Semiconductor	1×1	4.58	2.85	[63]
Bi(111)	Metal	1×1, $\sqrt{3} \times \sqrt{3}$R30	4.54	4	[47]
MoS_2	Semiconductor			2.9	[78]
Au(111)	Metal	2×2, $\sqrt{3} \times \sqrt{3}$, r3 $\times \sqrt{7} -> 1 \times 2$ of stanene $\sqrt{7}$	5.1–5.7	2.4 2.4	[68] [64]
$\sqrt{3} \times \sqrt{3}Au_2Sn$(111)	Metal	1×1	5.1	0.72	[71]
Ag(111)	Metal	$\sqrt{3} \times \sqrt{3}$	4.98	2.6	[57]

sandwiched between PbI_2 layers. In a follow-up paper [96], the group also showed that the QSHE is present in the same structure. Ni *et al.* [97] investigated PbI_2 and CaI_2 by means of DFT. They found both substrates to support stanene. While on PbI_2, it exhibits a trivial band gap; on CaI_2, it is metallic, but external strain can open a nontrivial band gap.

4.2.5 WS_2

Chen *et al.* [43] investigated theoretically stanene on WS_2 (see Figure 3d). They examined the interlayer distance, strain, and the influence of an external electric field on the system. The system is stable, above a certain interlayer distance, and the electronic structure has a band gap with a Dirac cone at the K point. The authors further show that the size of the band gap could be tuned with all the aforementioned parameters.

4.2.6 ZnO

Cao *et al.* [98] reported on their theoretical investigation of structural stability, as well as electronic and optical properties of a stanene/ZnO heterostructure. After finding the optimal interlayer distance, the electronic structure was determined to be metallic. A band gap can be opened, however, by the application of an electric field and by introducing strain. They also showed that the system has potentially high UV absorption capability.

4.2.7 Silicene

The interests of Noshin *et al.* [99] were directed to another elemental 2D material – silicene. The authors examined a stanene/silicene bilayer by DFT. Their focus was on investigating the thermal conductivity of the bilayer, and they showed that it has a thermal conductivity smaller than that of any other group IV elemental 2D material. Barhoumi *et al.* [100] showed in their DFT studies that a stanene/silicene bilayer is stable and the relaxed structure is a direct band gap semiconductor. It is important to note, however, that the lowest total energy was found for a set of two planar layers of Sn and Si, respectively, with the same lattice constant. The examined structure is therefore not a stack of typical, buckled stanene and silicene layers found in the literature.

4.2.8 BeO

Chakraborty *et al.* [101] investigated a stanene/BeO heterostructure. Its structural stability was confirmed, and electronic properties calculations showed a large band gap with Dirac cone opened, the size of which was enlarged by the interaction with the substrate.

4.2.9 TcS_2

In another paper, Barhoumi and Said [102] examined a technetium disulfide(TcS_2)/stanene heterostack for its electronic and vibrational properties. They found that the lowest energy structure is the T phase, which was confirmed to be dynamically stable by calculating its phonon spectra. Furthermore, the structure shows an indirect band gap of up to 1.4 eV.

4.2.10 Heterostacks of 2D materials

Yun *et al.* [103] investigated heterostacks of three 2D materials. Combinations of hBN/stanene/hBN, graphene/stanene/graphene and hBN/stanene/graphene were examined using DFT methods. Their studies revealed significant differences among the three stacks, closely dependent on lattice alignment. Only in the case of stanene sandwiched between two hBN layers, its electronic structure remains intact and it resembles an ideal monolayer. The Sn/C interaction was shown to involve strong electron transfer and close dependency on the alignment between the two lattices (Table 2).

5 Conclusions and outlook

In summary, the field of experimental synthesis of epitaxial stanene has many promises to realize and a number of obstacles to overcome. The main promise is a QSHE at room temperature, and all the possible utilizations of that effect in various devices. The main obstacle is synthesis. The consensus in the community is that freestanding stanene is not possible to realize, and techniques that would support the growth of some kind of supporting structure are necessary. The main technique utilized so far to create stanene is the epitaxial growth on a solid crystalline substrate.

While metallic substrates were used in early attempts to show that the synthesis of a stanene is possible, the

Table 2: Substrates proposed in DFT calculations

Substrate	Substrate band gap (eV)	Reconstruction	ε (%)	d (Å)	Δ (Å)	E_g (meV)	Z_2	Ref.
hBN	5	$1 \times 1/\sqrt{3} \times \sqrt{3}$	6.9	3.30	0.55–1.22	Up to 53	1	[28]
		$\sqrt{7} \times \sqrt{7}/5 \times 5$	1.5	3.3		3	1	[86]
		$3 \times 3/\sqrt{31} \times \sqrt{31}$R9	0.25	3.7–3.8		30		[87]
		$2 \times 2/4 \times 4$	7	3.4		93		[88]
		$2 \times 2/4 \times 4$	6	3.28–3.35				[103]
		$2 \times 2/4 \times 4$	5–8					
AlN	2.9	$1 \times 1/\sqrt{3} \times \sqrt{3}$	19.5	2.70	0.72	Semimetallic		[28]
		$2 \times 2/3 \times 3$	3.4	>4.00		63		[88]
		$2 \times 2/3 \times 3$	1	3				
Ge(111)	0.7	$\sqrt{3} \times \sqrt{3}/2 \times 2$	<1	3.2	1.4	34	1	[81]
		$\sqrt{3} \times \sqrt{3}/2 \times 2$	1.5					[91]
InSe	1.4 [104]	$\sqrt{3} \times \sqrt{3}/2 \times 2$	0.7	3.1		20		[94]
GaTe	1.65 [105]	$\sqrt{3} \times \sqrt{3}/2 \times 2$	2.2	3.45		80		[94]
α-Al_2O_3 (0001)	4.85 [106]	$1 \times 1/1 \times 1$	3	2.88	0.7–1.2	250	1	[44]
		$1 \times 1/1 \times 1$	2.7	2.7–2.9	1.18	260		[40]
		$1 \times 1/1 \times 1$	2.4	2.9		263		[45]
Ag(111)	—	7×7R19.107/$\sqrt{19} \times \sqrt{19}$R23.413	3.3	2.41–2.48	1.06	Metallic		[55]
		$4 \times 4/\sqrt{43} \times \sqrt{43}$R7.589	2.7	2.49				[38]
		$1 \times 1/\sqrt{3} \times \sqrt{3}$	4.38	1.81				
Au(111)	—	$1 \times 1/\sqrt{3} \times \sqrt{3}$	4.27	1.15	1.63	Metallic		[38]
		$\sqrt{7} \times \sqrt{7}/3 \times 3$				Metallic		[67]
Cu(111)	—	$1 \times 1/\sqrt{3} \times \sqrt{3}$	3.73	2.08	0.96	Metallic		[38]
Al(111)		$1 \times 1/\sqrt{3} \times \sqrt{3}$	3.83	2.49	1.08			
Pd(111)		$1 \times 1/\sqrt{3} \times \sqrt{3}$	1.25	2.31	0			
Pt(111)		$1 \times 1/\sqrt{3} \times \sqrt{3}$	1.81	2.37	0			
Ir(111)		$1 \times 1/\sqrt{3} \times \sqrt{3}$	0.38	2.36	0.01			
Ni(111)		$1 \times \sqrt{3}$R30/$2 \times 2\sqrt{3}$R30	4.15	2.30	0			
Graphene	—	$2 \times 2/4 \times 4$	4.7	3.3	0.8	80	0	[79]
Graphene/ stanene/graphene		$\sqrt{7} \times \sqrt{7}$R19.1/5×5	0.5	3.3	0.7–1.2	30	1	[80]
Graphene/ stanene/graphene		$\sqrt{7} \times \sqrt{7}/5 \times 5$	1.8	3.5–3.7	0.67	34		[82]
Graphene/SiC		$1 \times 1/2 \times 2$	5.1	3.3–4	0.79–1.26	15		[83]
		$1 \times 1/2 \times 2$	4.7	3.62	0.86	146		[103]
		$2 \times 2/4 \times 4$	5–8	3.73–5.39				[52]
		$\sqrt{7} \times \sqrt{7}$R19.1/$5 \times 5/4 \times 4$	0.28	3.32				
PbI_2	2.5	1×1	0.4	3.2	0.87	300	1	[95]
*(I-passivated stanene)		1×1	1.3	3.16	0.89	30	0	[96]
*Pristine stanene								[97]
MoS_2	1.8	$2 \times 2/3 \times 3$	1.28	3.2–3.4	0.85	72–77		[42]

(*Continued*)

Table 2: *Continued*

Substrate	Substrate band gap (eV)	Reconstruction	ε (%)	d (Å)	Δ (Å)	E_g (meV)	Z_2	Ref.
		$2 \times 2/3 \times 3$	1.45	3.1		67		[76]
		$2 \times 2/3 \times 3$	1.1	2.8		64		[77]
CaI_2	?	1×1	2.1	3.35	0.9	Metallic	1*	[97]
WS_2	1.8	$2 \times 2/3 \times 3$	1.9	3	0.85	62.9		[43]
ZnO	1.7	$2 \times 2/3 \times 3$	3.3	3	0.78	Metallic (60 at 3.2 A)		[98]
SiC (0001)	2.5	$2 \times 2/3 \times 3$	0.46	2.16	0.4–1.4s	Metallic	1	[51]
SiC (0001)-H		$2 \times 2/3 \times 3$	7.05	4.33		100	1	[41]
SiC (0001)-F		$2 \times 2/3 \times 3$	1	4.69		160		[54]
SiC monolayer		$2 \times 2/3 \times 3$	1	3.19–3.21		154–162		
SiC (0001)		$2 \times 2/3 \times 3$		2.0–2.7		23		
Silicene		$4 \times 4/5 \times 5$	0.6	3.4 5.2–5.5	0.83 0.0	70–160		[99] [100]
BeO	5	$2 \times 2/3 \times 3$	7	3	0.86	98		[101]
TcS_2	1.5			6.7–6.9		750–1370		[102]

*The Z_2 invariant on CaI_2 is unphysical due to stanene's semimetallic nature, but becomes physical when it becomes semiconducting by, *e.g.*, applying strain [97].

exotic properties of the 2D layer are inaccessible on such substrates, mainly due to too strong interaction between the materials. Hence, semiconducting and insulating substrates are in demand, with the first few works already reporting the successful synthesis. The early results are quite inspiring for further search of the "perfect" material, able to support stanene and preserve the properties predicted for its free-standing counterpart. Among the ones presented in our summary, it seems that semiconductors, such as MoS_2, InSb, and insulating hBN, are the materials studied the most intensively at the moment, with still room for exploration in the experimental field. An interesting approach may be also to use group IV elements in heterostacks, like in the first attempts to combine stanene with graphene or silicene, presented here. Finally, TMD materials may also be a good platform for the growth of stanene.

This review summarizes the substrates examined by theoretical calculations for their feasibility of supporting a stanene layer. It also includes many up-to-date reports on experimental realizations of stanene-like single layers of Sn. This report thus serves as a useful "orientation point" for researchers that are new in the field.

Funding information: This work is a part of the research program on 2D semiconductor crystals with Project No. FV157-TWOD, financed by the Netherlands Organization for Scientific Research (NWO).

Author contributions: All authors have accepted responsibility for the entire content of this manuscript and approved its submission.

Conflict of interest: The authors state no conflict of interest.

References

[1] Novoselov KS, Geim AK, Morozov SV, Jiang D, Katsnelson MI, Grigorieva IV, et al. Two-dimensional gas of massless Dirac fermsions in graphene. Nature. 2005;438:197–200.

[2] Zomer PJ, Dash SP, Tombros N, Wees BJvan. A transfer technique for high mobility graphene devices on commercially available hexagonal boron nitride. Appl Phys Lett. 2011;99:232104.

[3] Kane CL, Mele EJ. Quantum spin hall effect in graphene. Phys Rev Lett. 2005;95:226801.

[4] Yao Y, Ye F, Qi X-L, Zhang S-C, Fang Z. Spin–orbit gap of graphene: First-principles calculations. Phys Rev B. 2007;75:041401.
[5] Takeda K, Shiraishi K. Theoretical possibility of stage corrugation in Si and Ge analogs of graphite. Phys Rev B. 1994;50:14916–22.
[6] Guzmán-Verri GG, Lew Yan Voon LC. Electronic structure of silicon-based nanostructures. Phys Rev B. 2007;76:075131.
[7] Vogt P, Asensio MC, Resta A, Ealet B. Silicene: Compelling experimental evidence for graphenelike two-dimensional silicon. Phys Rev Lett. 2012;108:5.
[8] Fleurence A, Friedlein R, Ozaki T, Kawai H, Wang Y, Yamada-Takamura Y. Experimental evidence for epitaxial silicene on diboride thin films. Phys Rev Lett. 2012;108:245501.
[9] Kara A, Enriquez H, Seitsonen AP, Lew Yan Voon LC, Vizzini S, Aufray B, et al. A review on silicene – New candidate for electronics. Surf Sci Rep. 2012;67:1–18.
[10] Chowdhury S, Jana D. A theoretical review on electronic, magnetic and optical properties of silicene. Rep Prog Phys. 2016;79:126501.
[11] Houssa M, Pourtois G, Afanas'ev VV, Stesmans A. Electronic properties of two-dimensional hexagonal germanium. Appl Phys Lett. 2010;96:082111.
[12] Cahangirov S, Topsakal M, Aktürk E, Şahin H, Ciraci S. Two- and one-dimensional honeycomb structures of silicon and germanium. Phys Rev Lett. 2009;102:236804.
[13] Dávila ME, Xian L, Cahangirov S, Rubio A, Le Lay G. Germanene: a novel two-dimensional germanium allotrope akin to graphene and silicene. N J Phys. 2014;16:095002.
[14] Acun A, Zhang L, Bampoulis P, Farmanbar M, Houselt A, van, Rudenko AN, et al. Germanene: the germanium analogue of graphene. J Phys Condens Matter. 2015;27:443002.
[15] Kaloni TP, Schreckenbach G, Freund MS, Schwingenschlögl U. Current developments in silicene and germanene. Phys Status Solidi RRL - Rapid Res Lett. 2016;10:133–42.
[16] Liu N, Bo G, Liu Y, Xu X, Du Y, Dou SX. Recent progress on germanene and functionalized germanene: preparation, characterizations, applications, and challenges. Small. 2019;15:1805147.
[17] Xu Y, Yan B, Zhang H-J, Wang J, Xu G, Tang P, et al. Large-Gap Quantum Spin Hall Insulators in Tin Films. Phys Rev Lett. 2013;111:136804.
[18] Broek B, van den Houssa M, Scalise E, Pourtois G, Afanas'ev VV, Stesmans A. Two-dimensional hexagonal tin: *ab initio* geometry, stability, electronic structure and functionalization. 2D Mater. 2014;1:021004.
[19] Zhu F, Chen W, Xu Y, Gao C, Guan D, Liu C, et al. Epitaxial growth of two-dimensional stanene. Nat Mater. 2015;14:1020–5.
[20] Sahoo SK, Wei K-H. A perspective on recent advances in 2D stanene nanosheets. Adv Mater Interfaces. 2019;6:1900752.
[21] Lyu J, Zhang S, Zhang C, Wang P. Stanene: A Promising Material for New Electronic and Spintronic Applications. Ann Phys. 2019;531:1900017.
[22] Zhao C, Jia J. Stanene: A good platform for topological insulator and topological superconductor. Front Phys. 2020;15:53201.
[23] Ezawa M. Monolayer topological insulators: silicene, germanene, and stanene. J Phys Soc Jpn. 2015;84:121003.
[24] Molle A, Goldberger J, Houssa M, Xu Y, Zhang S-C, Akinwande D. Buckled two-dimensional xene sheets. Nat Mater. 2017;16:163–9.
[25] Liu C-C, Feng W, Yao Y. Quantum Spin Hall Effect in Silicene and Two-Dimensional Germanium. Phys Rev Lett. 2011;107:076802.
[26] Singh R. Spin–orbit splitting in graphene, silicene and germanene: Dependence on buckling. Int J Mod Phys B. 2018;32:1850055.
[27] Rivero P, Yan J-A, García-Suárez VM, Ferrer J, Barraza-Lopez S. Stability and properties of high-buckled two-dimensional tin and lead. Phys Rev B. 2014;90:241408.
[28] Wang D, Chen L, Wang X, Cui G, Zhang P. The effect of substrate and external strain on electronic structures of stanene film. Phys Chem Chem Phys. 2015;17:26979–87.
[29] Matthes L, Pulci O, Bechstedt F. Massive Dirac quasiparticles in the optical absorbance of graphene, silicene, germanene, and tinene. J Phys Condens Matter. 2013;25:395305.
[30] Tang P, Chen P, Cao W, Huang H, Cahangirov S, Xian L, et al. Stable two-dimensional dumbbell stanene: A quantum spin Hall insulator. Phys Rev B. 2014;90:121408.
[31] Liu C-C, Jiang H, Yao Y. Low-energy effective hamiltonian involving spin–orbit coupling in silicene and two-dimensional germanium and tin. Phys Rev B. 2011;84:195430.
[32] Mao Y, Long L, Xu C, Yuan J. First-principles study on the structure and electronic properties of stanane under electric fields. Mater Res Express. 2018;5:065023.
[33] Modarresi M, Kakoee A, Mogulkoc Y, Roknabadi MR. Effect of external strain on electronic structure of stanene. Comput Mater Sci. 2015;101:164–7.
[34] Fadaie M, Shahtahmassebi N, Roknabad MR. Effect of external electric field on the electronic structure and optical properties of stanene. Opt Quantum Electron. 2016;48:440.
[35] Ren C-C, Ji W-X, Zhang C-W, Li P, Wang P-J. The effects of biaxial strain and electric field on the electronic properties in stanene. Mater Res Express. 2016;3UNSP 105008.
[36] Zhang L, Qin W, Li L, Li S, Cui P, Jia Y, et al. Kinetic pathways towards mass production of single crystalline stanene on topological insulator substrates. Nanoscale. 2018;10:18988–94.
[37] Li J, Lei T, Wang J, Wu R, Zhao J, Zhao L, et al. Anisotropic electronic structure and interfacial chemical reaction of Stanene/Bi_2Te_3. J Phys Chem C. 2020;124:4917–24.
[38] Guo Y, Pan F, Ye M, Wang Y, Pan Y, Zhang X, et al. Interfacial properties of stanene–metal contacts. 2D Mater. 2016;3:035020.
[39] Yuhara J, Shichida Y. Epitaxial growth of two-dimensional Pb and Sn films on Al(111). Thin Solid Films. 2016;616:618–23.
[40] Araidai M, Kurosawa M, Ohta A, Shiraishi K. First-principles study on adsorption structure and electronic state of stanene on alpha-alumina surface. Jpn J Appl Phys. 2017;56:095701.
[41] Ferdous N, Islam MS, Park J, Hashimoto A. Tunable electronic properties in stanene and two dimensional silicon-carbide heterobilayer: A first principles investigation. Aip Adv. 2019;9:025120.
[42] Ren C-C, Feng Y, Zhang S-F, Zhang C-W, Wang P-J. The electronic properties of the stanene/MoS_2 heterostructure under strain. RSC Adv. 2017;7:9176–81.
[43] Chen X, Li Y, Tang J, Wu L, Liang D, Zhang R. First-principles study on electronic properties of stanene/WS_2 monolayer. Mod Phys Lett B. 2017;31:1750271.

[44] Wang H, Pi ST, Kim J, Wang Z, Fu HH, Wu RQ. Possibility of realizing quantum spin Hall effect at room temperature in stanene/A l 2 O 3 (0001). Phys Rev B. 2016;94:035112.
[45] Eltinge S, Ismail-Beigi S. Structure and binding of stanene on the Al2O3(0001) surface. ArXiv200900684 Cond-Mat [Internet]; 2020 Sep 1 [cited 2021 Sep 9]. http://arxiv.org/abs/2009.00684.
[46] Gou J, Kong L, Li H, Zhong Q, Li W, Cheng P, et al. Strain-induced band engineering in monolayer stanene on Sb(111). Phys Rev Mater. 2017;1:054004.
[47] Song Y-H, Wang Z-W, Jia Z-Y, Zhu X-Y, Shi Z-Q, Zhu L, et al. High-buckled 3×3 stanene with a topologically nontrivial energy gap. J Phys Appl Phys. 2021;54:304002.
[48] Zang Y, Jiang T, Gong Y, Guan Z, Liu C, Liao M, et al. Realizing an epitaxial decorated stanene with an insulating bandgap. Adv Funct Mater. 2018;28:1802723.
[49] Liao M, Zang Y, Guan Z, Li H, Gong Y, Zhu K, et al. Superconductivity in few-layer stanene. Nat Phys. 2018;14:344–8.
[50] Glass S, Li G, Adler F, Aulbach J, Fleszar A, Thomale R, et al. Triangular spin–orbit-coupled lattice with strong coulomb correlations: Sn atoms on a SiC(0001) substrate. Phys Rev Lett. 2015;114:247602.
[51] Matusalem F, Bechstedt F, Marques M, Teles LK. Quantum spin Hall phase in stanene-derived overlayers on passivated SiC substrates. Phys Rev B. 2016;94:241403.
[52] Matusalem F, Koda DS, Bechstedt F, Marques M, Teles LK. Deposition of topological silicene, germanene and stanene on graphene-covered SiC substrates. Sci Rep. 2017;7:15700.
[53] Di Sante D, Eck P, Bauernfeind M, Wil M, Thomale R, Schaefer J, et al. Towards topological quasifreestanding stanene *via* substrate engineering. Phys Rev B. 2019;99:035145.
[54] Li P. Stanene on a SiC(0001) surface: a candidate for realizing quantum anomalous Hall effect. Phys Chem Chem Phys. 2019;21:11150–7.
[55] Gao J, Zhang G, Zhang Y-W. Exploring Ag(111) substrate for epitaxially growing monolayer stanene: a first-principles study. Sci Rep. 2016;6:29107.
[56] Tao L, Cinquanta E, Chiappe D, Grazianetti C, Fanciulli M, Dubey M, et al. Silicene field-effect transistors operating at room temperature. Nat Nanotechnol. 2015;10:227–31.
[57] Yuhara J, Fujii Y, Nishino K, Isobe N, Nakatake M, Xian L, et al. Large area planar stanene epitaxially grown on Ag(1 1 1). 2D Mater. 2018;5:025002.
[58] Luh D-A, Wang C-H, Yang Y-W. Growth of thin Sn films on Ag (111) studied with low-energy electron diffraction and X-ray photoelectron spectroscopy. Thin Solid Films. 2019;682:44–9.
[59] Eguchi T, Nakamura J, Osaka T. Structure and electronic states of the α -Sn(111)-(2×2) Surface. J Phys Soc Jpn. 1998;67:381–4.
[60] Mason BF, Williams BR. Growth and recovery of a-Sn on InSb (OO1) using He scattering and LEED. Surf Sci. 1991;243:1–11.
[61] Fantini P, Mariani C, Sancrotti M. a-Sn pseudomorphic growth on InSb(111) and (111) surfaces: a high-resolution photoemission study. Surf Sci. 2000;9:174–82.
[62] Barfuss A, Dudy L, Scholz MR, Roth H, Höpfner P, Blumenstein C, et al. Elemental topological insulator with tunable fermi level: strained α-Sn on InSb(001). Phys Rev Lett. 2013;111:157205.
[63] Xu C-Z, Chan Y-H, Chen P, Wang X, Flötotto D, Hlevyack JA, et al. Gapped electronic structure of epitaxial stanene on InSb(111). Phys Rev B. 2018;97:035122.
[64] Maniraj M, Stadtmüller B, Jungkenn D, Düvel M, Emmerich S, Shi W, et al. A case study for the formation of stanene on a metal surface. Commun Phys. 2019;2:12.
[65] Deng J, Xia B, Ma X, Chen H, Shan H, Zhai X, et al. Epitaxial growth of ultraflat stanene with topological band inversion. Nat Mater. 2018;17:1081–6.
[66] Saxena S, Chaudhary RP, Shukla S. Stanene: Atomically thick free-standing layer of 2D hexagonal tin. Sci Rep. 2016;6:31073.
[67] Nigam S, Gupta S, Banyai D, Pandey R, Majumder C. Evidence of a graphene-like Sn-sheet on a Au(111) substrate: electronic structure and transport properties from first principles calculations. Phys Chem Chem Phys. 2015;17:6705–12.
[68] Liu Y, Gao N, Zhuang J, Liu C, Wang J, Hao W, et al. Realization of strained stanene by interface engineering. J Phys Chem Lett. 2019;10:1558–65.
[69] Maniraj M, Jungkenn D, Shi W, Emmerich S, Lyu L, Kollamana J, et al. Structure and electronic properties of the (3×3) R 30 ◦ SnA u 2/Au (111) surface alloy. Phys Rev B. 2018;98:205419.
[70] Pang W, Nishino K, Ogikubo T, Araidai M, Nakatake M, Le Lay G, et al. Epitaxial growth of honeycomb-like stanene on Au(111). Appl Surf Sci. 2020;517:146224.
[71] Zhou D, Li H, Bu S, Xin B, Jiang Y, Si N, et al. Phase engineering of epitaxial stanene on a surface alloy. J Phys Chem Lett. 2021;12:211–7.
[72] Ahmed R, Nakagawa T, Mizuno S. Structure determination of ultra-flat stanene on Cu(111) using low energy electron diffraction. Surf Sci. 2020;691:121498.
[73] Chiappe D, Scalise E, Cinquanta E, Grazianetti C, Broek B, van den, Fanciulli M, et al. Two-Dimensional Si nanosheets with local hexagonal structure on a MoS_2 surface. Adv Mater. 2014;26:2096–101.
[74] Bremen R, van Yao Q, Banerjee S, Cakir D, Oncel N, Zandvliet HJW. Intercalation of Si between MoS_2 layers. Beilstein J Nanotechnol. 2017;8:1952–60.
[75] Zhang L, Bampoulis P, Rudenko AN, Yao Q, Houselt A, van, Poelsema B, et al. Structural and electronic properties of germanene on MoS 2. Phys Rev Lett. 2016;116:256804.
[76] Liang D, He H, Lu P, Wu L, Zhang C, Guan P, et al. Tunable band gaps in stanene/MoS2 heterostructures. J Mater Sci. 2017;52:5799–806.
[77] Xiong W, Xia C, Du J, Wang T, Peng Y, Wei Z, et al. Band engineering of the MoS2/stanene heterostructure: strain and electrostatic gating. Nanotechnology. 2017;28:195702.
[78] Chen K-C. Multi-layer elemental 2D materials: antimonene, germanene and stanene grown directly on molybdenum disulfides. Semicond Sci Technol. 2019;34:8.
[79] Chen X, Meng R, Jiang J, Liang Q, Yang Q, Tan C, et al. Electronic structure and optical properties of graphene/stanene heterobilayer. Phys Chem Chem Phys. 2016;18:16302–9.
[80] Wu L, Lu P, Bi J, Yang C, Song Y, Guan P, et al. Structural and electronic properties of two-dimensional stanene and graphene heterostructure. Nanoscale Res Lett. 2016;11:525.

[81] Fang Y, Huang Z-Q, Hsu C-H, Li X, Xu Y, Zhou Y, et al. Quantum spin hall states in Stanene/Ge(111). Sci Rep. 2015;5:14196.
[82] Yun FF, Cortie DL, Wang XL. Tuning the electronic structure in stanene/graphene bilayers using strain and gas adsorption. Phys Chem Chem Phys. 2017;19:25574–81.
[83] Mondal C, Kumar S, Pathak B. Topologically protected hybrid states in graphene-stanene-graphene heterojunctions. J Mater Chem C. 2018;6:1920–5.
[84] Wu H, Tang J, Liang Q, Shi B, Niu Y, Si J, et al. A van der Waals epitaxial growth of ultrathin two-dimensional Sn film on graphene covered Cu(111) substrate. Appl Phys Lett. 2019;115:141601.
[85] Yang X, Ta HQ, Li W, Mendes RG, Liu Y, Shi Q, et al. In-situ observations of novel single-atom thick 2D tin membranes embedded in graphene. Nano Res. 2021;14:747–53.
[86] Wang M, Liu L, Liu C-C, Yao Y. van der Waals heterostructures of germanene, stanene, and silicene with hexagonal boron nitride and their topological domain walls. Phys Rev B. 2016;93:155412.
[87] Khan AI, Chakraborty T, Acharjee N, Subrina S. Stanene-hexagonal boron nitride heterobilayer: Structure and characterization of electronic property. Sci Rep. 2017;7:16347.
[88] Yelgel C. Tunable electronic properties of van der Waals heterostructures composed of stanene adsorbed on two-dimensional, graphene-like nitrides. J Appl Phys. 2019;125:155301.
[89] Dong X, Zhang L, Yoon M, Zhang P. The role of substrate on stabilizing new phases of two-dimensional tin. 2D Mater. 2021;8:045003.
[90] Chaudhary RP, Saxena S, Shukla S. Optical properties of stanene. Nanotechnology. 2016;27:495701.
[91] Bachra ME, Zaari H, Benyoussef A, Kenz AE, Hachimi AGE. First-principles calculations of van der waals and spin orbit effects on the two-dimensional topological insulator stanene and stanene on Ge(111) substrate. J Supercond Nov Magn. 2018;31:2579–88.
[92] Carpinelli JM, Weitering HH, Bartkowiak M, Stumpf R, Plummer EW. Surface Charge Ordering Transition: a Phase of $S\bar{n}Ge(111)$. Phys Rev Lett. 1997;79:4.
[93] Tejeda A, Cortés R, Lobo-Checa J, Didiot C, Kierren B, Malterre D, et al. Structural origin of the Sn 4 d core level line shape in Sn/Ge (111) – (3 × 3). Phys Rev Lett. 2008;100:026103.
[94] Ding Y, Wang Y. Quasi-Free-Standing Features of Stanene/Stanane on InSe and GaTe Nanosheets: A Computational Study. J Phys Chem C. 2015;119:27848–54.
[95] Zhang H, Zhou T, Zhang J, Zhao B, Yao Y, Yang Z. Quantum anomalous Hall effect in stanene on a nonmagnetic substrate. Phys Rev B. 2016;94:235409.
[96] Zhang H, Wang Z, Xu X. Room temperature quantum spin Hall insulator: Functionalized stanene on layered PbI2 substrate. Appl Phys Lett. 2017;111:072105.
[97] Ni Z, Minamitani E, Ando Y, Watanabe S. Germanene and stanene on two-dimensional substrates: Dirac cone and Z 2 invariant. Phys Rev B. 2017;96:075427.
[98] Cao H, Zhou Z, Zhou X, Cao J. Tunable electronic properties and optical properties of novel stanene/ZnO heterostructure: First-principles calculation. Comput Mater Sci. 2017;139:179–84.
[99] Noshin M, Khan AI, Subrina S. Thermal transport characterization of stanene/silicene heterobilayer and stanene bilayer nanostructures. Nanotechnology. 2018;29:185706.
[100] Barhoumi M, Lazaar K, Said M. DFT study of the electronic and vibrational properties of silicene/stanene heterobilayer. Phys E-Low-Dimens Syst Nanostructures. 2019;111:127–9.
[101] Chakraborty B, Borgohain MM, Adhikary NC. Structural and electronic properties of Stanene-BeO heterobilayer. Mater Res Express. 2020;7:015029.
[102] Barhoumi M, Said M. Electronic and vibrational properties of TcS2 and TcS2/Stanene heterobilayer using density functional theory. Phys E Low-Dimens Syst Nanostructures. 2020;124:114380.
[103] Yun FF, Cortie DL, Wang XL. Interactions in stanene centred van der Waals trilayers structures of boron-nitride and graphene: effect of mirror symmetry on electronic interactions. J Phys Condens Matter. 2020;32:265001.
[104] Politano A, Campi D, Cattelan M, Ben Amara I, Jaziri S, Mazzotti A, et al. Indium selenide: an insight into electronic band structure and surface excitations. Sci Rep. 2017;7:3445.
[105] Fonseca JJ, Tongay S, Topsakal M, Chew AR, Lin AJ, Ko C, et al. Bandgap restructuring of the layered semiconductor gallium telluride in air. Adv Mater. 2016;28:6465–70.
[106] Chen MX, Zhong Z, Weinerts M. Designing substrates for silicene and germanene: First-principles calculations. Phys Rev B. 2016;94:075409.